Mapping of Temperatures from Coarser to Finer Grid Using Temporal Derivatives

Mentor: Ravindra Akarapu, *Corning Incorporated*

Ilona Ambartsumyan, *University of Pittsburgh*

Cuiyu He, *Purdue University*

Eldar Khattatov, *University of Pittsburgh*

Sewoong Kim, *Pohang University of Science and Technology*

Lidia Mrad, *Purdue University*

Abstract

In many practical situations encountered in industries, there is incomplete knowledge of material properties, boundary conditions, and sources for a given material/manufacturing process. However, process monitors such as thermocouples are typically used to measure temperature evolution in certain locations to bridge the resulting gaps. Spatial gradients of temperature are needed to predict required quantities such as internal stresses developed during the process. The temperature measurements are typically performed on a coarse grid. Computation of stresses needs temperatures on a much finer grid for a more precise estimation of spatial gradients. Usually bilinear and/or weighted interpolation techniques are used to improve the spatial resolution of temperatures. However, in the cases where there are strong exothermic and/or endothermic reactions occurring during the process, such interpolation techniques are error-prone. Using more thermocouples to measure temperature on finer grid would be an easy solution. However, such measurement is intrusive as well as perturbing in addition to increasing the cost of data acquisition. The mapping of temperatures from coarser grid to finer grid is an ill-posed problem. In addition to the spatial distribution temperatures, the thermocouple measurements also contain valuable temporal information in the form of derivatives. This additional information of temporal derivatives helps in improving the conditioning of the apparently ill-posed problem. The objective of this project is to develop an algorithm/procedure for mapping temperatures from coarse grid to a finer grid recognizing as well as the valuable temporal information in the corresponding derivatives.

I. Introduction

In many industrial manufacturing processes, complete knowledge of material properties and information such as boundary conditions, sources/sinks is rarely available. However, process monitors such as thermocouples are installed to measure process parameters such as temperature. Usually, the temperature measurement is done at certain spatial locations inside the part or domain of interest. In the process of interest, we are interested in computation of stresses using the measured temperatures as loading. This involves computation of temperature gradients; which needs information of temperature on a finer grid. In a nut shell, the problem at hand is to map temperatures from a coarser grid to a finer grid (Fig. 1).

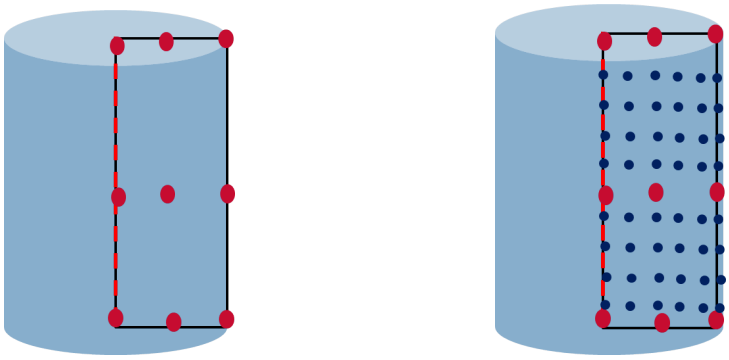

Figure 1: Coarse and Fine Grids

Interpolation based techniques are usually used for such mapping problems. However, in the presence of strong exothermic/ endothermic reactions, like the process of interest in this study, such interpolation techniques are error prone. To illustrate the point, let us illustrate a scenario. Let us say Fig. 2 shows the location of thermocouples. Measurements were made at locations "A" and "B". The temperature as function of time at these two location is given in Fig. 3 . Location "D" is midway between locations "A" and "B". The temperature evolution at location "D" was computed by interpolating temperatures at "A" and "B"; when compared to actual measurement (Fig. 4), the interpolation technique seems to be erroneous. Mapping of temperatures from coarse grid to fine grid is an ill-posed problem that falls into the category of inverse heat transfer problems.

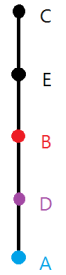

Figure 2: Location of Thermcouples

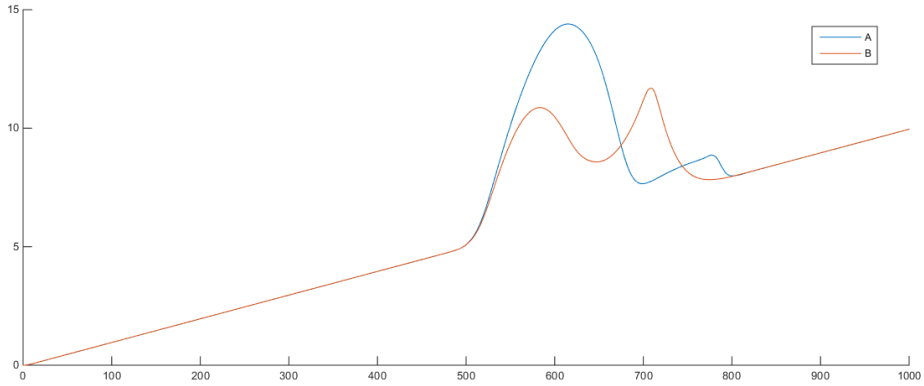

Figure 3: Measured Temperature

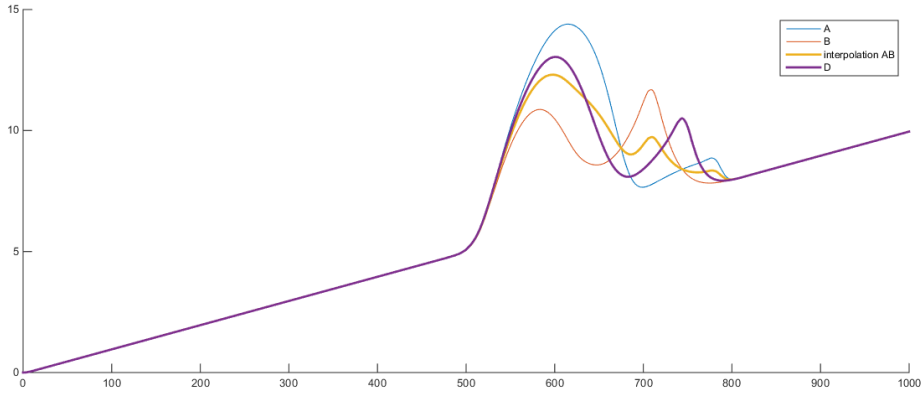

Figure 4: Interpolation

Inverse heat conduction problems, unlike direct problems, are usually ill-posed because low random errors in measurements can lead to large errors in identifications. There are several methods used to solve these problems. Some of them require the solution of the associated direct problem, while others don't. In this project, we adopt one method from each category. We have to point out that some published papers consider point or line heat sources [4] while others consider the heat source as a continuous function in a considered region [3]. Among the latter group of papers, some assume the heat source to be time-dependent only [8], and others assume it is only space dependent [9]. In our case, we do not have any restrictions on the form of heat source, other than being continuous in space and time.

Various numerical methods have been used for this inverse problem. Boundary methods can be used and are divided into two groups: boundary element methods [4] and the method of fundamental solutions [5]. Our first approach will apply the latter coupled with the use of radial basis functions. Note that this method does not require to solve the direct problem. The method of fundamental solutions (MFS) is a meshless method that was first proposed in the 60ies by Kupradze and Aleksidze. The solution is approximated by linear combinations of fundamental

solutions in terms of singularities placed on a fictitious boundary lying outside the physical domain. In [3], the authors employed this method to recover heat source in steady heat conduction problems. In [3], the problem is solved using the apriori information that the source is harmonic or satisfies Helmholtz equation. In our main reference for this approach [5], the authors use MFS with discretization of time derivative by $\theta-$method.

Another way to deal with the inverse problem is to use optimization approach, however, due to the ill-posedness of the problem one should be carefull with choosing the method to minimize the cost functional. One way to do so is to construct an iterative process using Conjugate Gradient method using the adjoint problem to compute the direction of the descent. There are four common techniques that can be put into this category, see Chapter 2 in [6]. The fact that the source function changes both in time and in space leads us to applying technique 4: the Conjugate Gradient method with Adjoint Problem for function estimation. The power of this technique is that it assumes no a priori information about the source function while the computation cost is the same or even less than the other techniques. Due to it using no prior information on the function one may doubt its efficiency in case of a complicated source function which unfortunately happens in our case. Our second step tackles the problem through a totally opposite direction. Instead of being totally blind about the source function, we assume that we know everything about the exact expression of the source function up to 1 unknown parameters. Under this circumstance, we apply the Newton's Method in 1D. It turns out that Newton's 1D method is very powerful to find the correct parameter.

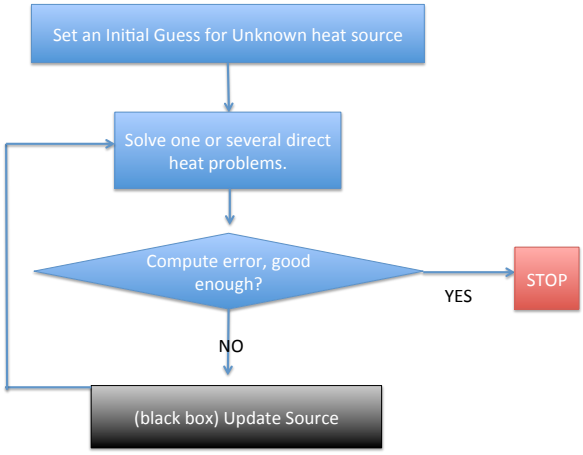

Figure 5: Flow chart for the iterative process.

Other methods were discussed and applied in literature such as finite difference method for time and finite element method for space discretizations [10], finite difference with discrete mollification method [11], and other special methods [1].

II. Mathematical Model

Our problem can be formulated as a heat equation with unknown temperature T and source term Q as follows:

$$\frac{\partial T(x,y,t)}{\partial t} - \triangle T(x,y,t) = Q(x,y,t) \qquad \text{in } \Omega \times [0,T] \tag{1}$$

$$T(x,y,0) = G(x,y) \qquad \text{in } \Omega \tag{2}$$

$$aT(x,y,t) + b\frac{\partial T(x,y,t)}{\partial n} = c \qquad \text{on } \partial\Omega \times [0,T] \tag{3}$$

where $Q(x,y,t)$ is an unknown moving heat source. The domain Ω is a two-dimensional rectangular domain, $\partial\Omega$ is its boundary. Eq. (2) is the initial condition and (3) is the mixed Neumann and Dirichlet boundary conditions.

The measured temperature by the thermocouples placed inside the cylinder provides an additional condition for our system:

$$T(x_i,y_i,t) = g_i(t) \qquad \text{for} \{(x_i,y_i)\}_{i=1}^{N} \quad \text{in } \Omega \tag{4}$$

III. First Approach

As mentioned before, the aim of this project is to move from a coarse grid where we know the measured temperature, to a finer grid. For that we need to solve the Inverse Heat Conduction Problem, keeping in mind that finding the heat source itself is not our main interest. We propose two different approaches to realize this goal.

In the first approach, we employ the method of fundamental solutions (MFS) along with the use of radial basis functions (RBFs) [5]. This numerical-analytical formulation exploits the fact that we can find an analytical solution of the proposed problem. In particular, the solution is approximated by a linear combination of fundamental solutions in terms of singularities (source points) placed on a fictitious boundary lying outside the domain. The unknown right-hand side is approximated by the use of radial basis functions. For the approximation of the time derivative, we use a finite difference method.

For this approach, we consider only Dirichlet boundary conditions:

$$T(x,y,t) = a \qquad \text{on } \partial\Omega \times [0,T] \tag{5}$$

1. Method of Fundamental Solutions

We outline the method as follows. For a finite difference method, we choose the θ-method. Let τ be the time increment and $t_n = n\tau$ for $n \geq 1$. Approximate:

$$T(x,y,t) \approx \theta.T(x,y,t_n) + (1-\theta)T(x,y,t_{n-1})$$
$$\frac{\partial T(x,y,t)}{\partial t} \approx \frac{T(x,y,t_n) - T(x,y,t_{n-1})}{\tau}$$

where $0 \leq \theta \leq 1$.
Substituting in (1),

$$\frac{T(x,y,t_n) - T(x,y,t_{n-1})}{\tau} - \theta.\Delta T(x,y,t_n) - (1-\theta)\Delta T(x,y,t_{n-1}) = Q(x,y,t_{n-1}).$$

Denote $T(x,y,t_n)$ by $w_n(x,y)$. Then

$$\frac{w_n - w_{n-1}}{\tau} - \theta.\Delta w_n - (1-\theta)\Delta w_{n-1} = Q_{n-1}.$$

Rearranging terms,

$$\Delta w_n - \frac{1}{\theta.\tau} w_n = -\frac{1}{\theta.\tau} w_{n-1} - \frac{(1-\theta)}{\theta}\Delta w_{n-1} - \frac{1}{\theta} Q_{n-1} \tag{6}$$

which is the modified Helmholtz equation. At each time step t_n, w_{n-1} and Δw_{n-1} could be obtained from the previous time step but note that Q_{n-1} is unknown. Hence the right-hand side of the modified Helmholtz equation is an unknown function $f_{n-1}(x,y)$ and that's how we'll treat it in this specific algorithm.

We write the solution of (6) as the sum of the homogeneous solution $w_n^{(h)}$ and a particular solution $w_n^{(p)}$, i.e. $w_n = w_n^{(h)} + w_n^{(p)}$, where these solutions satisfy the following independent Helmholtz equations respectively:

$$\Delta w_n^{(h)} - \lambda^2 w_n^{(h)} = 0 \tag{7}$$

$$\Delta w_n^{(p)} - \lambda^2 w_n^{(p)} = f_n \tag{8}$$

where $\lambda = \dfrac{1}{\theta.\tau}$. The approximate solution of Eq. (6) is a superposition of fundamental solutions of the modified Helmholtz equation with unknown coefficients W_j:

$$w_n^{(h)}(x,y) = \sum_{j=1}^{NS} W_j K_0(\lambda\sqrt{(x-x_j)^2 + (y-y_j)^2}) \tag{9}$$

where K_0 is a modified Bessel function of the second kind and zero order and (x_j, y_j) are coordinates of source points located outside the region Ω.

2. Radial Basis Functions

To find a particular solution, we use radial basis functions to approximate the right-hand side [7]. To that effect, we start by writing $f_n(x,y)$ as

$$f_n(x,y) = \sum_{m=1}^{M} \alpha_m \hat{\varphi}(r_m)$$

where α_m are the unknowns and the radial basis functions $\hat{\varphi}$ are chosen to be the thin plate spline centered at (x_m, y_m); $\hat{\alpha}(r_m) = r_m^2 \ln(r_m)$. The linear system provided by this interpolation condition could be ill-posed, for example if $\{(x_i, y_i)\}_{i=2}^{M}$ lie on the ball of center (x_1, y_1). Fortunately, it can be shown that it is suitable to add a polynomial of degree $K \geq 1$ to fix this. The extra degrees

of freedom are usually taken up by moment conditions on the coefficients $(\alpha_m)_{m=1}^M$. The theory guarantees the existence of one vector $(\alpha_m)_{m=1}^M$ and a unique polynomial satisfying the resulting system [7]. Thus the right hand-side is written as

$$f_n(x_i, y_i) = \sum_{m=1}^{M} \alpha_m \hat{\varphi}(r_{mi}) + \sum_{k=1}^{K} \beta_k \widetilde{\varphi}_k(x_i, y_i) \qquad 1 \leq i \leq M$$

where $r_{mi} = \sqrt{(x_i - x_m)^2 + (y_i - y_m)^2}$ and the moment condition

$$\sum_{m=1}^{M} \alpha_m \widetilde{\varphi}_k(x_m, y_m) = 0.$$

Now we can express the particular solution of the non-homogeneous modified Helmholtz equation in the form:

$$w_n^{(p)}(x, y) = \sum_{m=1}^{M} \alpha_m \hat{\psi}(r_m) + \sum_{k=1}^{K} \beta_k \widetilde{\psi}_k(x, y) \tag{10}$$

where $\hat{\psi}(r_m)$ and $\widetilde{\psi}_k$ are solutions of non-homogeneous Helmholtz equation with the corresponding radial basis function and monomial on the right-hand side respectively.

$$\Delta\hat{\psi}(r_m) - \lambda^2 \hat{\psi}(r_m) = \hat{\varphi}(r_m) \tag{11}$$

$$\Delta\widetilde{\psi}_k(x, y) - \lambda^2 \widetilde{\psi}_k(x, y) = \widetilde{\varphi}_k(x, y) \tag{12}$$

The above equations have analytical solutions given by:

$$\hat{\psi}(r_m) \begin{cases} -\frac{4}{\lambda^4}[K_0(\lambda . r_m) + \ln(r_m) + 1] - \frac{r_m^2 \ln(r_m)}{\lambda^2} & \text{for } r_m > 0 \\ \frac{4}{\lambda^4}[\gamma_{\text{euler}} + \ln(\frac{\lambda}{2}) - 1] & \text{for } r_m = 0 \end{cases}$$

where $\gamma_{\text{euler}} = 0.57721$ is the Euler constant.
Monomials $\widetilde{\varphi}_k(x, y)$ and their particular solutions $\widetilde{\psi}_k(x, y)$ are given in the following table:

k	$\widetilde{\varphi}_k(x,y)$	$\widetilde{\psi}_k(x,y)$
1	1	$-\frac{1}{\lambda^2}$
2	x	$-\frac{x}{\lambda^2}$
3	y	$-\frac{y}{\lambda^2}$
4	xy	$-\frac{xy}{\lambda^2}$
5	x^2	$-\frac{x^2}{\lambda^2}-\frac{2}{\lambda^4}$
6	y^2	$-\frac{y^2}{\lambda^2}-\frac{2}{\lambda^4}$
7	x^3	$-\frac{x^3}{\lambda^2}-\frac{6x}{\lambda^4}$
8	x^2y	$-\frac{x^2y}{\lambda^2}-\frac{2y}{\lambda^4}$
9	xy^2	$-\frac{xy^2}{\lambda^2}-\frac{2x}{\lambda^4}$
10	y^3	$-\frac{y^3}{\lambda^2}-\frac{6y}{\lambda^4}$

Using the homogeneous solution (9) and the particular solution (10), now the solution of (6) can be written in the following form

$$\begin{aligned} w_n &= w_n^{(h)} + w_n^{(p)} \\ &= \sum_{j=1}^{NS} W_j K_0(\lambda r_j) + \sum_{m=1}^{M} \alpha_m \hat{\psi}(r_m) + \sum_{k=1}^{K} \beta_k \widetilde{\psi}_k(x,y) \end{aligned} \tag{13}$$

We need to construct a linear system to determine the unknown coefficients W_j, α_m and β_k in the following way. To apply this method, we split the points where we have measued data into two categories, M interior points, $\{(x_i,y_i)\}_{i=1}^{M}$ and NB boundary (collocation) points $\{(x_i,y_i)\}_{i=M+1}^{M+NB}$.

From the additional condition (4) obtained from the measured data at the interior points as shown in Fig. 6:

$$\sum_{j=1}^{NS} W_j K_0(\lambda r_{ji}) + \sum_{m=1}^{M} \alpha_m \hat{\psi}(r_{mi}) + \sum_{k=1}^{K} \beta_k \widetilde{\psi}_k(x_i,y_i) = T_i \qquad i =, 2, ..., M. \tag{14}$$

From the boundary condition (5) applied to the boundary points as shown in Fig. 6:

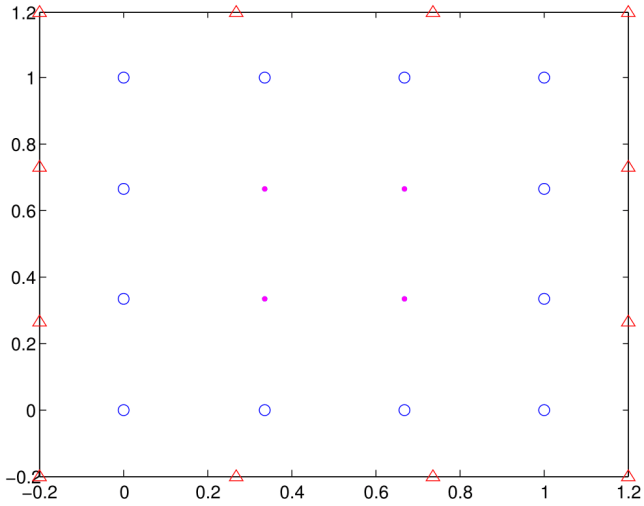

Figure 6: Location of boundary, source and interpolation points

$$\sum_{j=1}^{NS} W_j K_0(\lambda r_{ji}) + \sum_{m=1}^{M} \alpha_m \hat{\psi}(r_{mi}) + \sum_{k=1}^{K} \beta_k \widetilde{\psi}_k(x_i, y_i) = a_i \qquad i = M+1, 2, ..., M+NB. \tag{15}$$

Note that the above 2 equations come from the measured data in our case.
To complete the system, we add the moment condition

$$\sum_{m=1}^{M} \alpha_m \widetilde{\varphi}_k(x_m, y_m) = 0 \qquad k = 1, 2, ..., K. \tag{16}$$

Therefore we construct an algebraic system of $M + NB + K$ equations and $M + NS + K$ unknowns resulting from the unknown coefficients W_j, α_m and β_k. This can be written in a matrix form:

$$A\omega = b$$

where A is an $(M + NB + K) \times (M + NS + K)$ matrix, ω is a column vector of unknown coefficients W_j, α_m, β_k and b is a column vector containing the prescribed boundary, additional and interpolation conditions.

To avoid an ill-conditioned matrix A, we choose the source points NS to be the same as the boundary points NS as we have the flexibility to do so.

Once we solve the system, we get the expression of the temperature at *any* point inside the

domain at a specific time step:

$$T(x,y,t_n) = \sum_{j=1}^{NS} W_j K_0(\lambda r_j) + \sum_{m=1}^{M} \alpha_m \hat{\psi}(r_m) + \sum_{k=1}^{K} \beta_k \widetilde{\psi}_k(x,y).$$

Though it's not our main focus, but we also get the heat source expression:

$$Q(x,y,t_n) = -\theta \left(\alpha_m \hat{\psi}(r_m) + \sum_{k=1}^{K} \beta_k \widetilde{\psi}_k(x,y) \right) - \frac{1}{\tau} - (1-\theta)\Delta T(x,y,t_n)$$

3. Algorithm

First we construct the mesh from the points where the data is given $\{(x_i,y_i)\}_{i=1}^{N}$. This will give us NB boundary points and M interior points where $N = NB + M$. We choose $NS(= NB)$ source points outside the domain at a distance δ from the boundary points. Here we choose δ =0.2.
We also choose the time step τ and the parameter θ for the finite difference method.
From the data, we have the initial conditions T_0 we assume $\Delta T_0 = 0$

Algorithm:

1) For $n = 1$, $t_n = n.\tau$.

2) From the given data, for the boundary and interior points respectively, calculate

$$T_{B_n} = \sum_{j=1}^{NS} W_j K_0(\lambda r_{ji}) + \sum_{m=1}^{M} \alpha_m \hat{\psi}(r_{mi}) + \sum_{k=1}^{K} \beta_k \widetilde{\psi}_k(x_i,y_i) \qquad i =, 2, ..., M. \tag{17}$$

$$T_{INT_n} = \sum_{j=1}^{NS} W_j K_0(\lambda r_{ji}) + \sum_{m=1}^{M} \alpha_m \hat{\psi}(r_{mi}) + \sum_{k=1}^{K} \beta_k \widetilde{\psi}_k(x_i,y_i) \qquad i = M+1, 2, ..., M+NB. \tag{18}$$

and the moment condition

$$0 = \sum_{m=1}^{M} \alpha_m \widetilde{\varphi}_k(x_m,y_m) = 0 \qquad k = 1, 2, ..., K. \tag{19}$$

3) Solve the resulting linear system $A\omega = b$.

4) Calculate T_n, the right-hand side f_{n-1}, source functions Q_{n-1} and $\Delta T = f_n(x,y) + \frac{1}{\theta.\tau} T_n$.

5) Increment and go to step 2).

A Note on how to obtain 3D equivalent Algorithm:

The above method outlines an algorithm for a 2D domain, which is our main interest. We can, however, obtain an equivalent 3D algorithm based on solving 3D Helmholtz equations using compactly supported Radial Basis Functions (CS-RBFs) as in [2]. This reference outlines how to get solutions to Helmholtz-type equations $Lu = f$, where L is a radially and translationally invariant operator such as $\Delta - s^2 I$. For Wedland's CS-RBF $\varphi = r\left(1 - \frac{r}{a}\right)_+^2$ as a right-hand side, the solution is of the following form:

$$\psi(r)\begin{cases} s(2B+q(0))+q'(0) & \text{for } r=0 \\ \dfrac{Ae^{-sr}+Be^{sr}+q(r)}{r} & \text{for } 0<r\le a \\ \dfrac{Ce^{-sr}}{r} & \text{for } r>a \end{cases}$$

where

$$\begin{aligned} q(r) &= \frac{4}{s^4a}-\frac{1}{s^2}r-\frac{6}{s^4a^2}r+\frac{2}{s^2a}r^2-\frac{1}{s^2a^2}r^3 \\ A &= -\frac{e^{-as}(3+as)+4as}{s^5a^2} \\ B &= \frac{e^{as}(3+as)}{s^5a^2} \\ C &= \frac{3e^{as}-e^{as}(3+as)-as(4+e^{as})}{s^5a^2} \end{aligned}$$

4. Results

In order to validate the proposed numerical method, we carried out several 2D numerical examples. All test-cases are formulated on unit square $\Omega=[0,1]\times[0,1]$, the distance between contour of the boundary and the contour of sources equals 0.1, and the time increment $\tau=0.001$. In order to get a square linear system on each time step, we set the number of source points to be equal to the number of collocation points $NS=NB$. Note, that since our initial goal was to recover the temperature values, we don't discuss the approximation of the right-hand side function.
We first consider several examples with the form of function of heat generation as well as exact solutions are known (see Table 1). Corresponding values of temperature inside of the domain and boundary conditions, used in the algorithm, result from the exact form of solution.

	Solution	Source function
1st	$t\frac{(x-6)^3+(y-6)^3}{6}$	$\frac{x^3+y^3}{6}-3(x^2+y^2)+18(x+y-4)-t(x+y-12)$
2nd	$(1-4e^{-4t})(\cos(2x)+\cos(2y))$	$4(\cos(2x)+\cos(2y))$
3rd	$\sin(x)\sin(y)\sin(t)$	$\sin(x)\sin(y)(2\sin(t)+\cos(t))$

Table 1: The sources function and analytical solution of test examples

1) In the first case the true solution is a linear function of time and our method handles it even with small number of measurements and monomials in expansion for the right-hand side of the system. Here we consider $M=4$ uniformly distributed points inside the domain and $NB=12$ points on the boundary, with $K=3$ monomials. Fig. 7 shows the analytical and

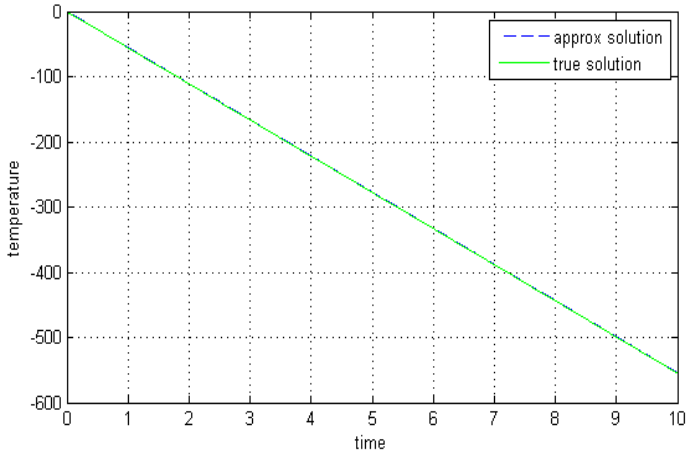

Figure 7: Analytical and numerical solutions for point $x = 0.2, y = 0.3$ for the 1st test case

numerical solutions for a point $x = 0.2, y = 0.3$. As we can see the graphs coincide visually and the corresponding relative error is $\frac{\|T_{tr} - T_{num}\|_{l_2}}{\|T_{tr} - T_{num}\|_{l_2}} = 1.8e - 3$

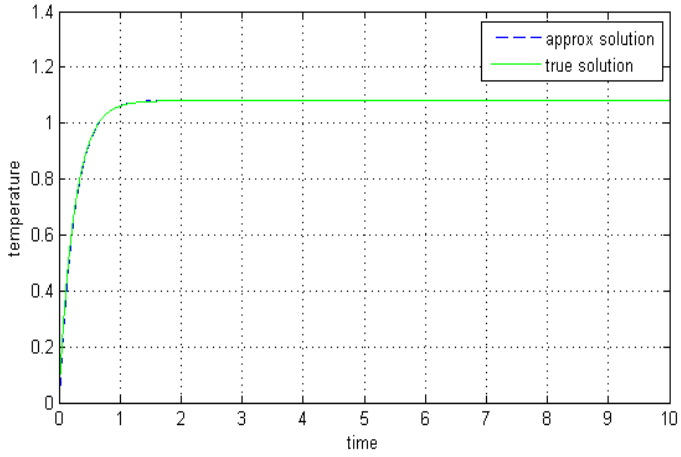

Figure 8: Analytical and numerical solutions for point $x = 0.2, y = 0.3$ for the 2nd test case

2) For the second test case our method also works in the same setting. Comparison between true and approximate solutions is given on Fig.8 and the relative error in this case is $4.7e - 3$

3) In our last example, the method shows worse results with chosen parameters - the relative error is $1.5e - 01$ and we see the discrepancy between the graphs on Fig.9a. Increasing the number of measurement and collocation points we reduce the error to $1.8e - 2$ and the graphs now agree (see Fig.9b)

All these examples show that the method works and now we are ready to run several test cases with data close to experimental.

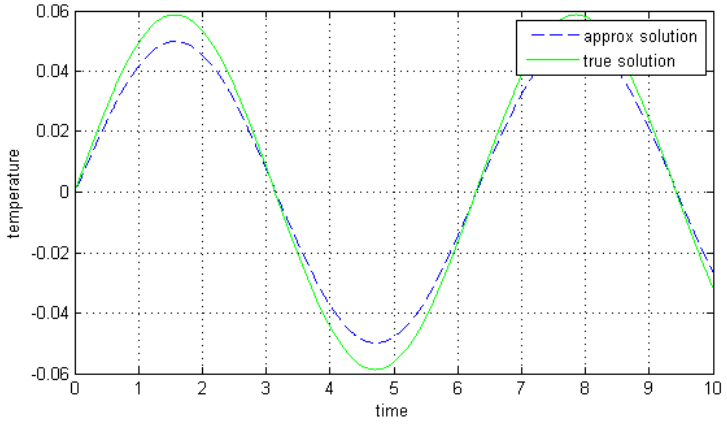

(a) $M = 4, NB = 12$

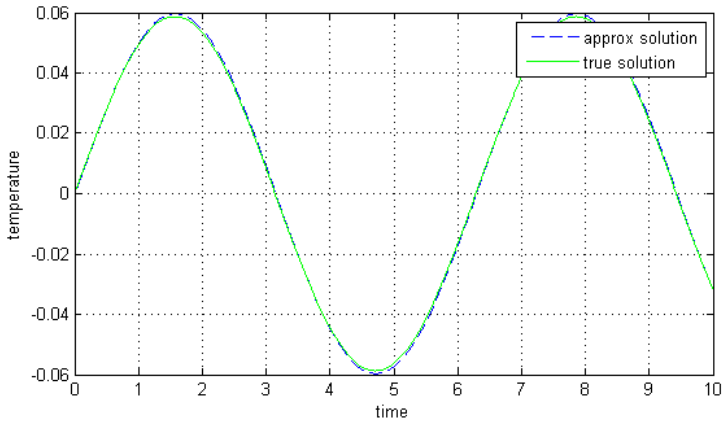

(b) $M = 16, NB = 20$

Figure 9: Analytical and numerical solutions for point $x = 0.2, y = 0.3$ for the 3rd test case

Now we don't have analytical solutions, so in order to verify the results, obtained using our model, we first generated different sets of data for points inside of the domain and on the boundary, and then we used some of these values to compute the solution for the rest of the points. In all test cases we use the source function of the form

$$Q(x, y, t) = q_0 \exp(-2\frac{y - (z_0 - v_0 t)^2}{w_0^2}),$$

where q_0, z_0, v_0, w_0 are some fixed coefficients. As one can see, changing these parameters, we can obtain a Gaussian function with very small support and high amplitude. We tested three sets of values, presented in the Table 2.

1) In the first test case we consider the data corresponding to a source function, which moves from the top to the bottom of the domain in time. The corresponding parameters are relatively mild, so the support of the source function is not very small and the amplitude is not very big.

	Parameters
1^{st}	$q_0 =, z_0 =, v_0 =, w_0 =$
2^{nd}	$q_0 =, z_0 =, v_0 =, w_0 =$
3^{rd}	$q_0 =, z_0 =, v_0 =, w_0 =$

Table 2: Parameters for the right-hand side function

We started with $M = 24$ points inside of the domain and $NB = 24$ points on the boundary. As one can see from Fig.10a the solutions do not coincide and the approximate solution doesn't have the right shape. So we increase the number of measurements and collocation points to $M = 42$, $NB = 30$. In this case the solutions are close to each other and the relative error is $3.8e - 03$

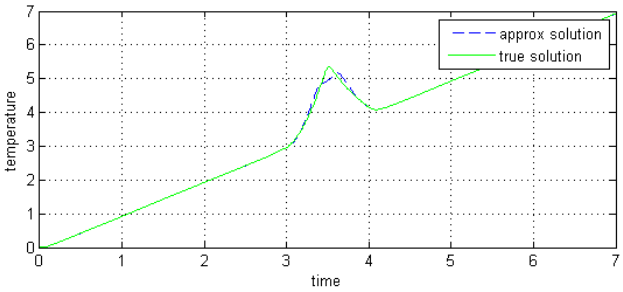

(a) $M = 24, NB = 24$

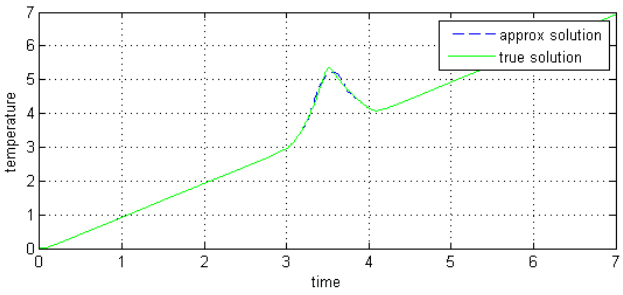

(b) $M = 42, NB = 30$

Figure 10: True and approximate solutions for the test case with mild parameters

2) In the second test case we still assume that the source function moves from the top to the bottom of the domain, but we consider a tougher set of parameters. Comparison between true and approximate solutions is given on Fig.11. Here we again start with $M = 24$ and $NB = 24$ and then add points inside of the domain and on the boundary in order to obtain a better result. When $M = 42$, $NB = 30$, the relative error is $3.4e - 02$

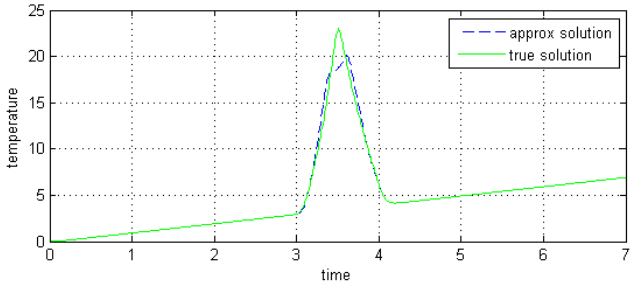

(a) $M = 24, NB = 24$

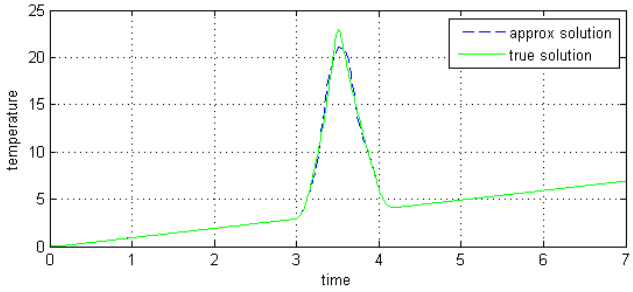

(b) $M = 42, NB = 30$

Figure 11: True and approximate solutions for the test case with mild parameters

3) Finally, in the third example, we assume that the force moves from the three sides inside the domain, while the fourth side is fixed. As before, we present two results: with $M = 24$, $NB = 24$ and $M = 42$, $NB = 30$ (see Fig.12). For this case the relative error is $3.9e - 03$

Recall that our main goal was to obtain fine spatial data, with accuracy at least higher than using bilinear interpolation. So, to verify that described method meets our needs, we present comparison between computed solutions and solutions obtained by using interpolation.

As we can see from Fig.13 computed values are closer to the actual solution than the interpolation, moreover the numerical solution has a shape close to the true one, while the interpolation produces two peaks instead of one.

We conclude that the method indeed provides a good approximation of unknown values. Its main disadvantage is that in order to get a high accuracy we need a lot of measurements, which is not realistic within the framework of our problem.

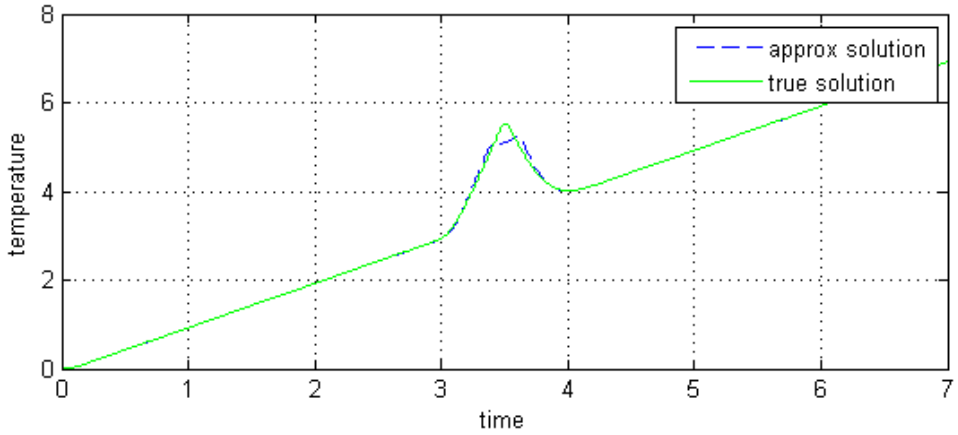

(a) $M = 24, NB = 24$

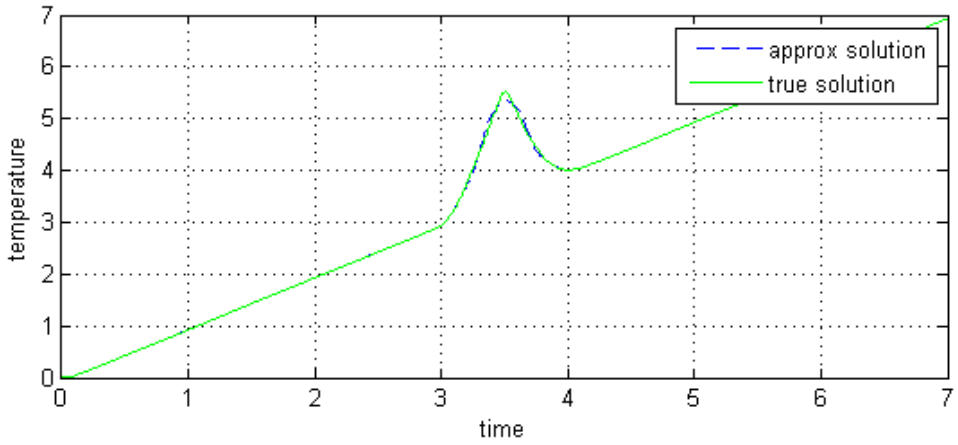

(b) $M = 42, NB = 30$

Figure 12: True and approximate solutions for the test case with mild parameters

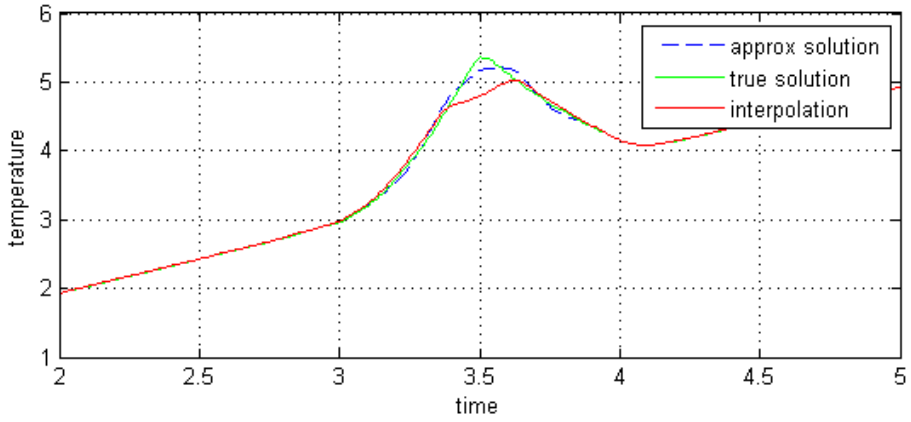

(a) 1st test case

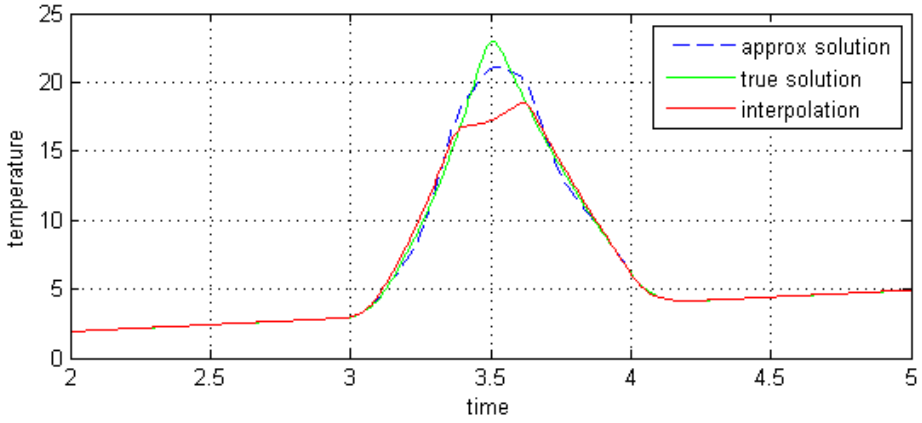

(b) 2nd test case

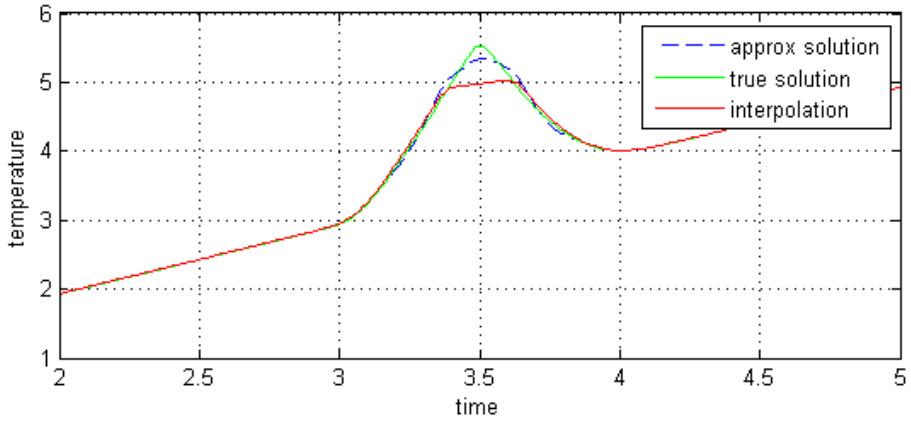

(c) 3rd test case

Figure 13: Numerical solutions and interpolation

IV. Second Approach

1. CG method.

In order not to confuse readers, we restate our model problem in 1D here. To this end, all analysis and numerical experiments will be based on the 1D model problem. However, I need to point out that extending results in this section to the 2D dimensions is straightforward.

$$\begin{cases} \dfrac{\partial T(x,t)}{\partial t} - \dfrac{\partial^2 T(x,t)}{\partial x^2} = G(x,t) & \text{in } [0\ M] \times [0\ T], \\ T(M,t) = g_0(t) & t \in [0\ T], \\ \dfrac{\partial T(0,t)}{\partial n} = 0 & t \in [0\ T], \\ T(x,0) = 0 & x \in [0\ M], \end{cases} \tag{20}$$

where X is the maximal length of the spacial domain and T is the maximal time length. The heat source $G(x,t)$ is unknown. The available measurements(data) are phrased as follows:

$$T(x_i,t) = g_i(t), \qquad i = 1, 2, \cdots, M,$$

where M is the number of sensors and x_i is the location of sensors. In our test problem, we will consider 5 sensors in total.

We first introduce the objective functional which measures the error as the difference between estimated solution and provide measurements.

$$S(G) = \sum_{i=1}^{M} \int_0^T [g_i(t) - T(x_i,t,G)]^2 \, dt,$$

with $T(x,t,G)$ being the temperature given heat source $G(x,t)$.

We now present the details for each step regarding CG method applied to our test problem, one can refer [6] for more details.

The Direct Problem

The direct problem is concerned with the determination of the temperature field $T(x,t)$ when the source function $G^0(x,t)$ is given. The superscript 0 is used to indicate that it is only an initial guess of the heat source for the current iteration.

The Sensitivity Problem

The sensitivity problem is described as follows:

$$\begin{cases} \dfrac{\partial \triangle T(x,t)}{\partial t} - \dfrac{\partial^2 \triangle T(x,t)}{\partial x^2} = \triangle G(x,t) & \text{in } [0\ M] \times [0\ T], \\ T(M,t) = 0 & t \in [0\ T], \\ \dfrac{\partial T(0,t)}{\partial n} = 0 & t \in [0\ T], \\ T(x,0) = 0 & x \in [0\ M], \end{cases} \tag{21}$$

where $\triangle G$ is a small perturbation for the heat source. The sensitivity problem determines the perturbation of temperature under some source perturbation $\triangle G(x,t)$.

The Adjoint Problem

In order to minimize the objective functional, we need to introduce a Lagrange multiplier $\lambda(x,t)$ because $T(x,t,G)$ actually need to satisfy the constraint of heat equation. We write the extended objective functional as follows:

$$S(G) = \sum_{i=1}^{M} \int_0^T (g_i(t) - T(x_i,t,G))^2\, dt + \int_{x=0}^{X} \int_{t=0}^{T} \lambda(x,t) \left(-\frac{\partial T(x,t)}{\partial t} + \frac{\partial^2 T(x,t)}{\partial x^2} + G(x,t) \right) dt\, dx.$$

We now replace G by a small perturbation $G + \triangle G$, T by $T + \triangle T$ in the above functional and subtract from it the original expression, we have

$$\begin{aligned} \triangle S(G) = \sum_{i=1}^{M} \int_0^T \int_{x=0}^{X} 2[T(x,t,G) - g_i(t)] \triangle T(x,t) \delta(x - x_i)\, dx\, dt \\ + \int_{x=0}^{X} \int_{t=0}^{T} \lambda(x,t) \left(-\frac{\partial \triangle T(x,t)}{\partial t} + \frac{\partial^2 \triangle T(x,t)}{\partial x^2} + \triangle G(x,t) \right) dt\, dx. \end{aligned}$$

Applying integration by parts to the second term, the above expression can be simplified to the following:

$$\begin{aligned} \triangle S(G) &= \sum_{i=1}^{M} \int_0^T \int_{x=0}^{X} \left(\frac{\partial^2 \lambda(x,t)}{\partial x^2} + \frac{\partial \lambda(x,t)}{\partial t} + 2[T(x,t,G) - g_i(t)] \triangle T(x,t) \delta(x - x_i) \right) \triangle T(x,t)\, dx\, dt \\ &+ \int_{t=0}^{T} \frac{\partial \triangle T(X,t)}{\partial x} \lambda(X,t) + \frac{\partial \lambda(0,t)}{\partial x} \triangle T(0,t)\, dt\, dx + \int_{x=0}^{X} \lambda(x,T) \triangle T(x,T)\, dx \\ &+ \int_0^T \int_{x=0}^{X} \lambda(x,t) \triangle G(x,t)\, dx\, dt \end{aligned}$$

The boundary value problem for the Lagrange multiplier $\lambda(x,t)$ is obtained by allowing the first

four integral terms to vanish. This leads to the following adjoint problem:

$$\begin{cases} \dfrac{\partial \lambda(x,t)}{\partial t} + \dfrac{\partial^2 \lambda(x,t)}{\partial x^2} + 2\sum_{i=1}^{M}(T(x,t) - g_i(t))\delta(x - x_i) = 0 \\ \lambda(X,t) = 0 \\ \dfrac{\partial \lambda(0,t)}{\partial n} = 0 \\ \lambda(x,T) = 0. \end{cases}$$

By making a change of variables $\tau = T - t$, and let $\hat{\lambda}(x,\tau) = \lambda(x,t)$, we have the following heat problem for $\hat{\lambda}$,

$$\begin{cases} \dfrac{\partial \hat{\lambda}(x,t)}{\partial t} - \dfrac{\partial^2 \hat{\lambda}(x,t)}{\partial x^2} = 2\sum_{i=1}^{M}(T(x,t) - g_i(t))\delta(x - x_i) \\ \hat{\lambda}(X,t) = 0 \\ \dfrac{\partial \hat{\lambda}(0,t)}{\partial n} = 0 \\ \hat{\lambda}(x,0) = 0. \end{cases}$$

Now we get

$$\triangle S(G) = \int_0^T \int_{x=0}^{X} \lambda(x,t) \triangle G(x,t)\, dx\, dt.$$

Algorithm

Let $G^0(x,t)$ be our initial guess for $G(x,t)$. Set $k = 0$, then:

1) Solve the direct problem (20) and get $T(x,t,G^k)$.
2) Check the stopping criteria
3) Solve the adjoint problem (22) and get $\lambda(x,t)$.
4) Set $\nabla S(G^k) = \lambda(x,t)$ and calculate γ_k as follows:

$$\gamma^k = \frac{\int\int \nabla S(G^k) \cdot (\nabla S(G^k) - \nabla S(G^{k-1}))dxdt}{\int\int \nabla S(G^{k-1})^2 dxdt}.$$

In case $k = 0$, set $\gamma_0 = 0$.

5) Calculate the optimal decent direction d^k:

$$d^k(x,t) = \nabla S(G^k) + \gamma^k d^{k-1}(x,t).$$

6) Set $\triangle G(x,t) = d^k(x,t)$, solve the sensitivity problem (21) and compute $\triangle T(x,t,d^k)$.

7) Calculate the step size β^k:

$$\beta^k = \frac{\sum_{i=1}^{M} \left(\int_0^T T^k(x_i,t) - g_i(t) \right) \triangle T(x_i,t,d^k) dt}{\sum_{i=1}^{M} \int_0^T \triangle T^k(x_i,t,d^k)^2 dt}.$$

8) Finally, update the source function by the following rule:

$$G^{k+1}(x,t) = G^k(x,t) - \beta^k d^k(x,t).$$

9) Set $k = k+1$ and return to step 1.

Results

In this section we start with providing the numerical results for several test cases in 1D. Our computational domain is the unit interval, shown on the figure (ref). We start with getting the set of "measurments" by solving the direct heat conduction problem with particular source function, and we try to recover this function from measurements afterwards. We use the following boundary and initial conditions:

$$\begin{aligned} T(0,t) &= g_0(t), && \text{where } g_0(t) \text{ is the measurement} \\ T(1,t) &= g_N(t), && \text{where } g_N(t) \text{ is the measurement} \\ T(x,0) &= 0 \end{aligned}$$

Next, knowing the "measurements" at only three points, see figure (ref) we would try to estimate the values at the points in between those. In all of the experiments, the tolerance of the Conjugate Gradient method is set to be relatively high $tol = 10e-1$, this was done to speed up the algorithm.

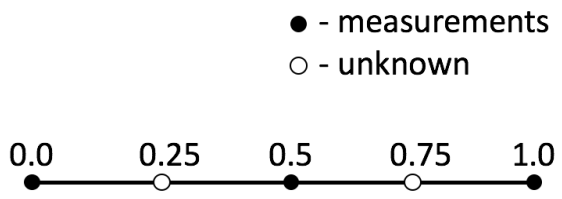

Figure 14: Computational domain

We do three test cases with the source functions given in the table 3. It is important to mention, that while test cases 1 and 2 are used to show that the described method works, the last test case 3 actually represents the physical problem we are working on - it was experimentally shown, that the source function in test case #3 may indeed describe the processes occuring in the ceramic filters in the kiln. We use the FEniCS software package [12] to implement the finite element method for the direct heat equation. We provide the numerical results in figures (15) - (20) and the errors in table 4.

Table 3: Source functions used in numerical experiments

Test case	Source function
#1	$10 * \exp\left(-(x-0.5)^2\right) \exp\left(-(t-1)^2\right)$
#2	$10 * \sin\left(x\,t\right)$
#3	$400 * \exp\left(\frac{-2(x-(4-2t))^2}{0.0025}\right)$

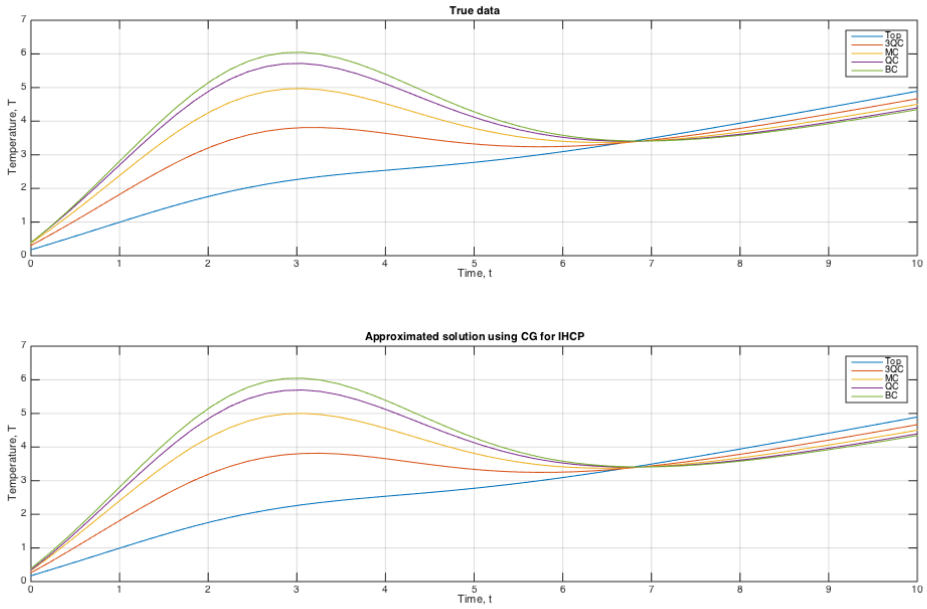

Figure 15: Measured and computed temperatures at 5 points, case #1

While the figures and errors show that the CG method yields very decent approximation to the unknown source function, and hence unknown temperatures at inner points, we have to admit that it is not suitable for the needs of this project for several reasons:

1) It is very computationally expensive on the fine grid - the method requires 3 solves of the heat equation per each CG iteration. This is not a problem for 1D case, however for the 2D and 3D cases it will require a lot of computational power and time since we need to keep mesh fine enough due to the nature of the source functions;

2) It does not resolve the peaks accurately - the ability to obtain the peak in the temperature evolution at a given point is the most important requirement the we had in this project, unfortunately this method smothens those peaks, see figure 20;

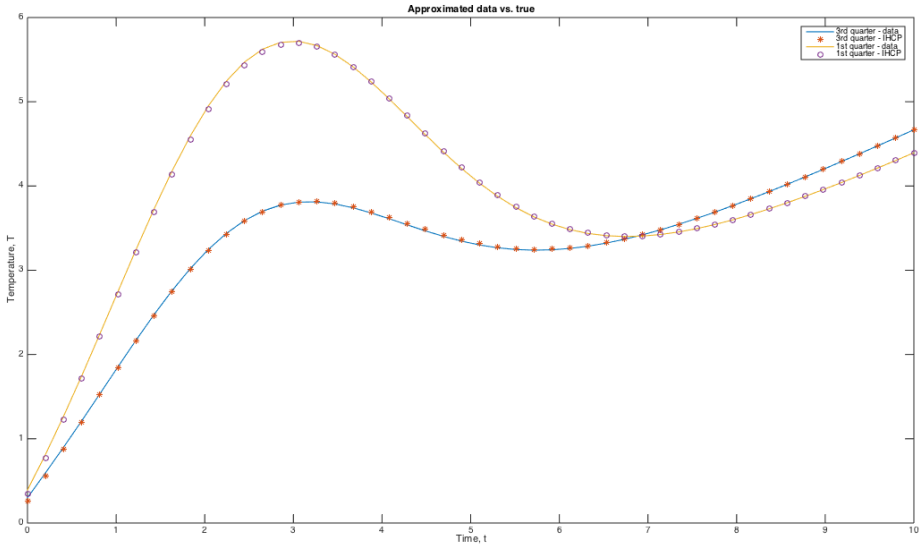

Figure 16: Measurements and computed temperatures at points of interest, case #2

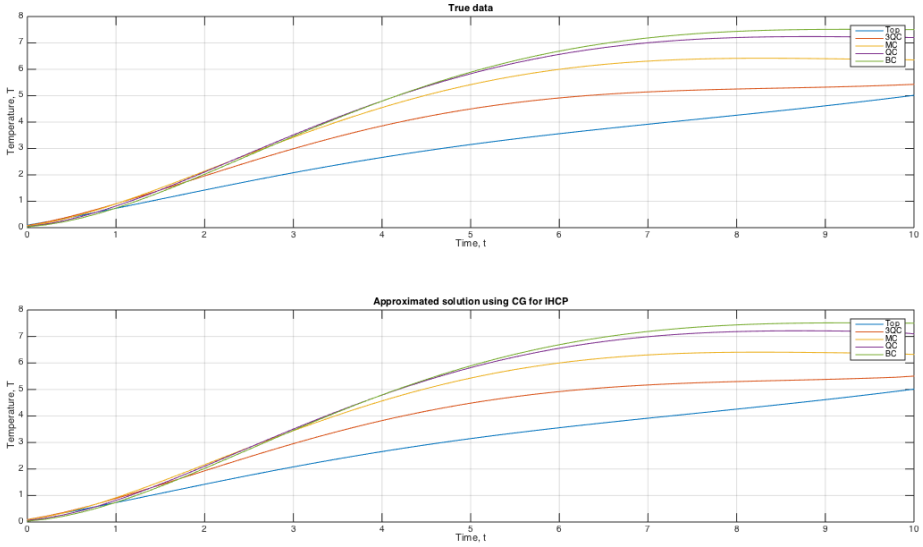

Figure 17: Measured and computed temperatures at 5 points, case #2

3) It yields worse accuracy, than the method of fundamental solutions.

Due to the aforementioned reasons, we decided not to extend our experiments to the 2D and 3D cases.

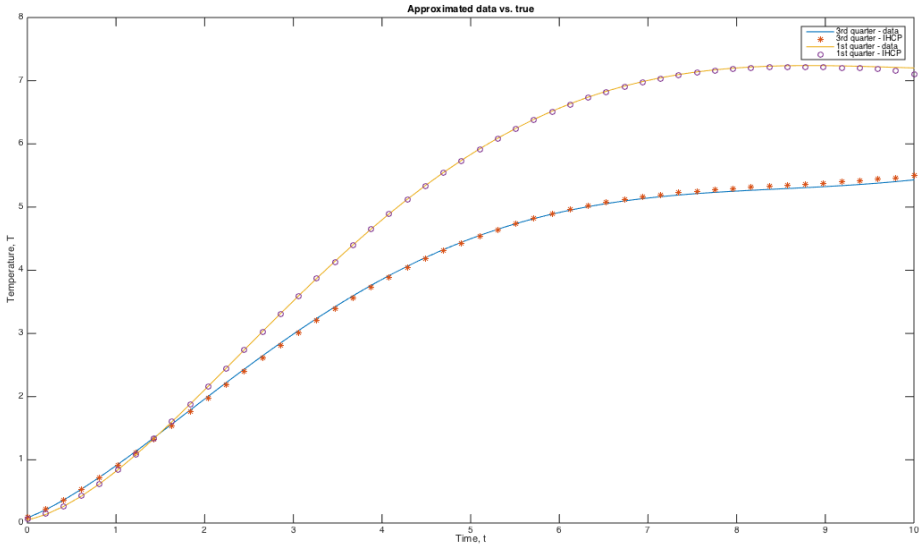

Figure 18: Measurements and computed temperatures at points of interest, case #2

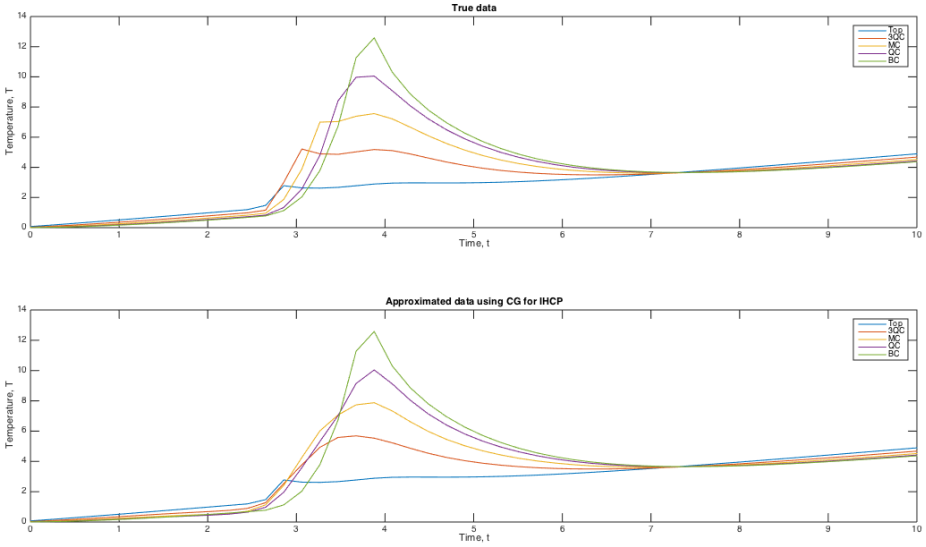

Figure 19: Measured and computed temperatures at 5 points, case #3

2. Newton's method in 1D.

In this section, we will assume that our source function has the expression

$$G(x,t) = 400 * \exp\left((-100 * w_0^2 * (x - x_0 + v_0 * t)^2)\right)$$

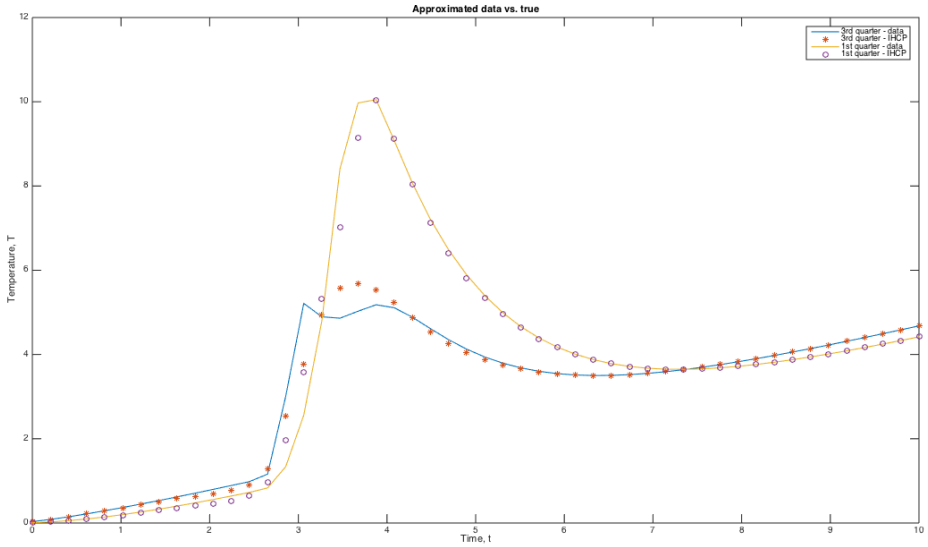

Figure 20: Measurements and computed temperatures at points of interest, case #3

Table 4: Relative errors between measured and computed temperatures

Test case	Relative error
#1	$2.1849e-3$
#2	$8.8320e-3$
#3	$7.7103e-2$

where w_0, x_0 and v_0 are a unknown parameters. The value we set for test problem is

$$w_0 = \sqrt{8}, x_0 = 4, \text{and } v_0 = 2.$$

Newton's Method in 1D.

Start with the simpliest case and assuming that two of the three parameters can be estimated accurately from the data, we only need to determine the one that is left. If this is the case, we will use Newton's Method in 1D. Newton's method is an iterative method for finding the roots of a differentiable function. The following figure illustrate the iterative process for this method in 1D.

In our case, it is easy to observe the fact that our objective function $S(p)$ equals zeros when $P = P_0$.

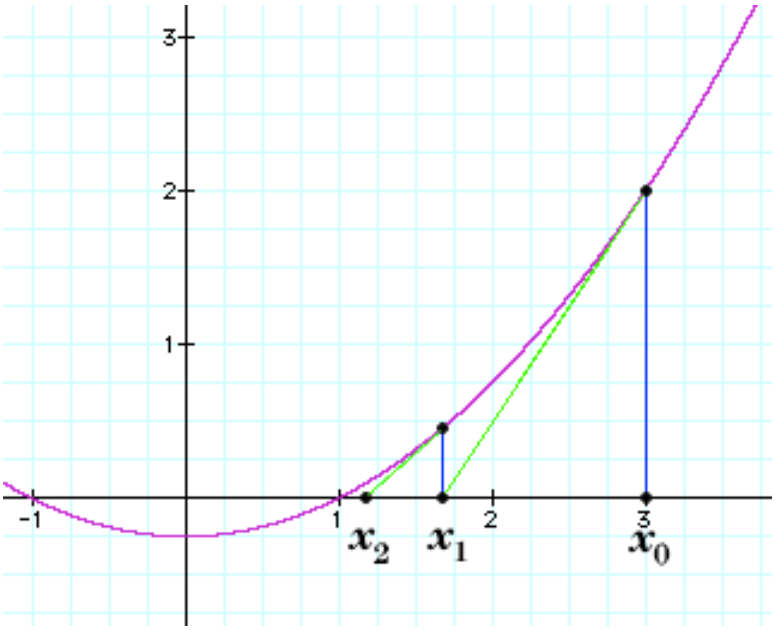

Figure 21: Graphical reasoning behind Newton's method

Algorithm

Without loss of generality, we assume that w_0 is the only unknown. Listed as follows is a brief Algorithm for Newton's Method in 1D applying to IHCP for one parameter estimation.

1) Set an initial guess for w_0; set $k = 0$;

2) Solve the direct heat problem (20) and compute $T(x, t, w_0)$ and $S(w_0)$.

3) Set $w = w_0 + 0.01$, solve the direct heat problem (20) and compute $T(x, t, w)$ and $S(w)$.

4) Compute the slope by

$$\text{slope} = \frac{S(w) - S(w_0)}{0.01}.$$

5) Compute the update

$$w_0 = w_0 - \frac{S(w_0)}{\text{slope}}.$$

. Set $k = k + 1$, and go to step 1.

Remark:

- In the above process, two direct heat problems are solved in each iterative procedure.
- The slope is a approximation since we do not know the exact form of $S(w)$.

Results

In order to get a visual comparison, we first provide two figures of accurate estimation of the true solution in the whole domain as well as on the measurement points.

Figure 22: True Solution

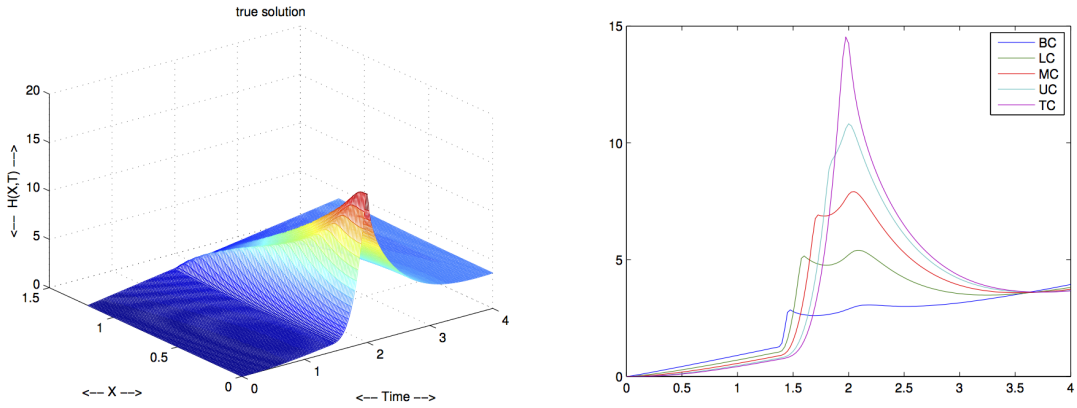

In the following figures, the left upper one is the final temperature estimation both in x dimension and t dimension. The right upper one is the final temperature at the measurement point. The lower left one is the iterative value for the unknown parameter. The lower right one is the iterative cost.

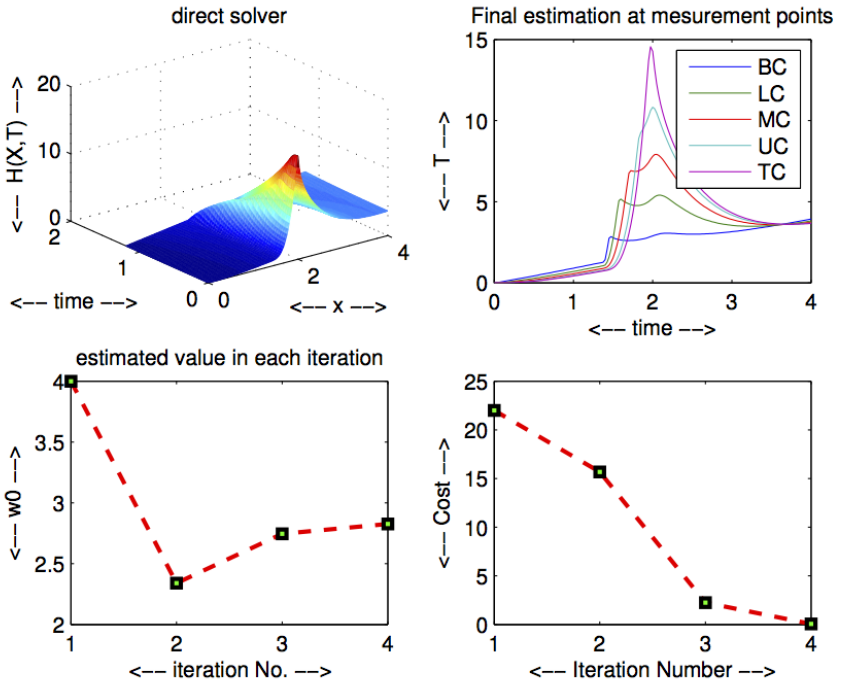

Figure 23: Newton's Method in 1D to determine w_0.

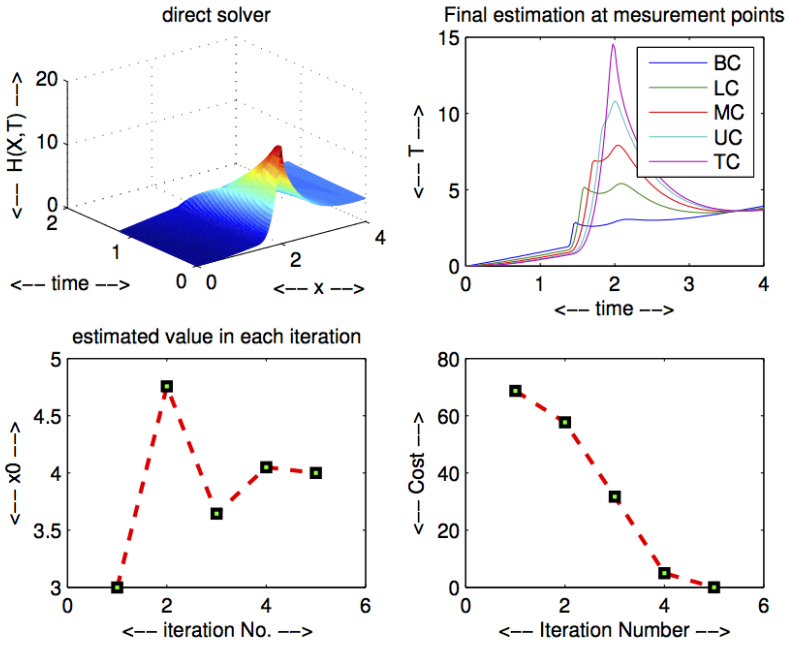

Figure 24: Newton's Method in 1D to determine x_0.

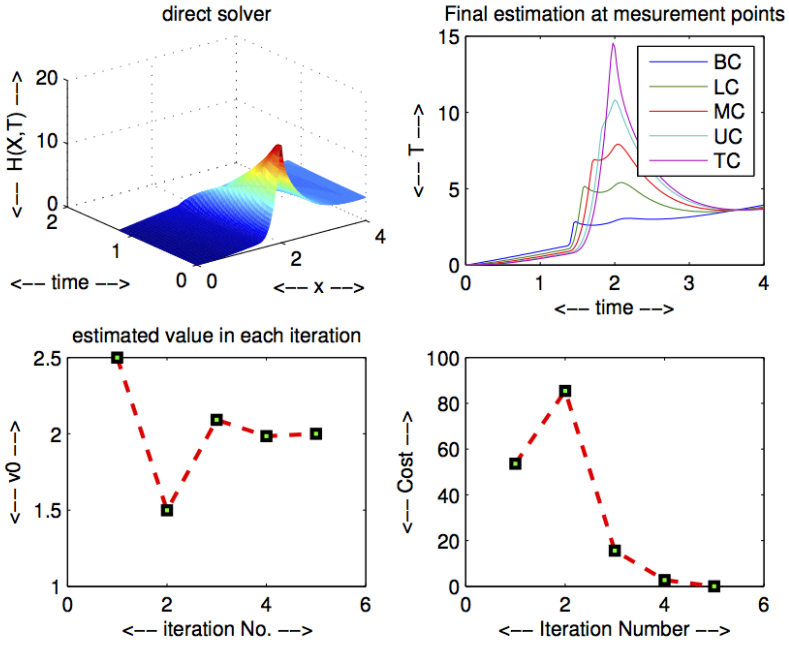

Figure 25: Newton's Method in 1D to determine v_0.

The measured data given in our test comes from a numerical approximation of the true source.

It turns out that Newton's Method is efficient in estimating each parameter. However, when we extend to Newton's Method in 3D intending to estimate 3 parameters simultaneously, the numerical results was not promising even the initial value is chosen to be very close to the true ones.

V. Conclusion

For the given problem we have implemented and compared two methods - the meshfree method of fundamental solutions and the conjugate gradient method for solving the inverse heat conduction problem. While not focusing on theoretical aspects of the aforementioned methods, we discussed their applicability to the problem of mapping of temperatures from coarser to finer grids, provided the very limited set of measurements. We compared the methods based on their accuracy, computational costs and extensibility to three-dimensional real-world problem. We have found that the method of fundamental solutions is better suited for this specific application, being both more accurate and computationally efficient compared to a more common optimizational approach based on conjugate gradient minimization method.

References

[1] Borukhov V.T., Kolesnikov P. M. , Method of Inverse Dynamic System and its Application for Recording Interval Heat Sources, *International Journal of Heat and Mass Transfer*, **31**, 8, (1998) 1549-1555.

[2] Goldberg M.A., Chen C. S., Ganesh M., Particular Solutions of 3D Helmholtz-type Equations Using Compactly Supported Radial Basis Functions, *Engineering Analysis with Boundary Elements*, **24**, (2000) 539-547.

[3] Jin B.. Marin L., The Method of Fundamental Solutions for Inverse Source Problems associated with the Steady-State Heat Conduction, *International Journal for Numerical Methods in Engineering*, **68**, 8, (2007) 1570-1589.

[4] Karami G., Hematiyan M.R., A Boundary Element Method for Inverse Non-linear Heat Conduction Analysis with Point Line and Heat Sources, *Communications in Numerical Methods in Engineering*, **16**, 2, (2000) 191-203.

[5] Mierwiczak M., Kolodziej J. A., Application of the Method of Fundamental Solutions and Radial Basis Functions for Inverse Transient Heat Source Problem, *Computer Physics Communications*, **181**, (2010) 2053-2043.

[6] M. Necati Özisik, Helcio R. B. Orlande INVERSE HEAT TRANSFER: FUNDAMENTALS AND APPLICATIONS, *Taylor & Francis, 2000.*

[7] Powell M. J. D., The Theory of Radial Basis Function Approximation in 1990, *Advances in Numerical Analysis II: Wavelets, Subdivision Algorithms and Radial Functions*, Oxford University Press, (1992) 105-210.

[8] Yan L., Fu C.-L., Yang F.-L., The Method of Fundamental Solutions for the Inverse Heat Source Problem, *Engineering Analysis with Boundary Elements*, **32**, 3, (2008) 216-222.

[9] Yan L., Yang F.-L., Fu C.-L., A Meshless Method for Solving an Inverse Spacewise-dependent Heat Source, *Journal of Computational Physics*, **228**, 1, (2009) 123-136..

[10] Yang C.-Y., Solving the Two-dimensional Inverse Heat Source Problem through the Linear Least-Squares Error Method, *International Journal of Heat and Mass Transfer*, **41**, 2, (1998) 393-398.

[11] Yi Zh., Murio D. A., Solving the Two-dimensional Inverse Heat Source Problem through the Linear Least-Squares Error Method, *International Journal of Heat and Mass Transfer*, **41**, 2, (2004) 393-398.

[12] A. Logg, K.-A. Mardal, G. N. Wells et al. (2012). Automated Solution of Differential Equations by the Finite Element Method, *Springer*.